Hindawi
Indoor Air
Volume 2024, Article ID 1537588, 12 pages
https://doi.org/10.1155/2024/1537588

Research Article

Indoor Air Remediation Using Biochar from Bark: Impact of Particle Size and Pollutant Concentration

Mariem Zouari,[1,2] **Silvo Hribernik**,[3] **and Matthew Schwarzkopf**[1,2]

[1]*InnoRenew CoE, Livade 6a, 6310 Izola, Slovenia*
[2]*Faculty of Mathematics, Natural Sciences, and Information Technologies, University of Primorska, Muzejski trg 2, 6000 Koper, Slovenia*
[3]*Faculty of Electrical Engineering and Computer Science, University of Maribor, Koroška cesta 46, 2000 Maribor, Slovenia*

Correspondence should be addressed to Mariem Zouari; mariem.zouari@innorenew.eu

Received 11 January 2024; Revised 25 March 2024; Accepted 26 March 2024; Published 16 April 2024

Academic Editor: Faming Wang

The growing emphasis on indoor air quality and public health is fuelling the need for efficient yet affordable air purification techniques. In this study, the influence of biochar particle size on its adsorption efficiency toward airborne pollutants was examined. Bark-derived biochar particles were treated by grinding or ball milling, and then, seven samples with different particle size groups were separated. Biochar particles were characterized by particle size, proximate, SEM, XRD, and physisorption analyses. For adsorption efficiency, two different pollutants were tested at variable initial concentrations. The physical composition and XRD patterns of the biochar with different particle sizes were comparable. The ball-milled sample was an exception in that it had higher ash content and additional XRD peaks signifying contamination of the sample. The porosity of biochar was greater in smaller particles. Ball milling increased the specific surface area and total pore volume by 102% and 48%, respectively. Biochar with finer particle size exhibited the highest adsorption potential towards formaldehyde and methanol among other samples. It should be emphasized that simple mechanical grinding is preferred for reducing biochar size to avoid the risk of eventual contamination, greater energy consumption, and slower processing related to ball milling. When a low concentration of pollutant was tested (1 ppm formaldehyde), the effect of particle size on the adsorption efficiency was more noticeable. However, the effect of particle size was less dominant when higher concentrations of pollutants were tested. Smaller biochar particles (<100 μm) are more favourable for indoor air remediation given their superior adsorption efficiency of volatile organic compounds occurring at low concentrations in the buildings.

1. Introduction

Exposure to indoor air pollution poses a major risk to human health. Reports from the World Health Organization stated that indoor air pollution is responsible for causing up to 3 million premature deaths per year worldwide [1]. A variety of airborne pollutants can be detected indoors, for example, volatile organic compounds (VOCs) which have been widely studied due to their harmful effect on human health. Exposure to indoor VOCs has been associated with occurrences of central nervous system failure, respiratory tract damage, visual disorder, cancer, etc. [2]. Hence, controlling indoor VOC levels is a key component to improve the air quality and mitigate the risk of diseases. One way to do that is by using simple, yet efficient air purification strategies such as adsorption on a porous material [3].

Current trends of sustainability and environmental awareness push toward the exploitation of underutilized organic feedstocks. Forest industry by-products such as wood chips, sawdust, and bark represent an abundant resource that is generated in large volumes. Bark is obtained after peeling or debarking logs in mills. Bark represents 6% to 20% of the total log volume [4] with an estimated amount of 23 million metric tons of available tree bark [5].

Bark components vary widely depending on tree species, tree age, and different bark layers. Due to the heterogeneous

composition and high content of impurities, the bark is usually used as a horticultural substrate [6] or managed by incineration for energy production [7]. However, the utilization of bark as an energy source is limited by its high ash content given that ash elements tend to decrease the heating value [8] and cause fouling problems in the combustors. For this reason, bark was not considered an adequate feedstock for energy production [9].

One treatment method that can increase the value of bark material is thermal conversion, specifically, slow pyrolysis. Slow pyrolysis consists of the decomposition of the original biomass under high heat and inert atmospheric conditions. Slow pyrolysis mainly yields a solid residue called biochar along with some condensable and noncondensable gases. The valorization of bark biomass to produce biochar represents a sustainable approach toward waste management and boosts the circular economy. Biochar is a renewable solid residue with high carbon content. It is characterized by high surface area, large pore volume, and the presence of surface functional groups [10]. These features make biochar a highly efficient adsorbent for use in the remediation of environmental contaminants including VOCs [11]. Biochar's chemical and physical properties vary with the original biomass type and the pyrolysis conditions (i.e., temperature and time) [12]. The properties of biochar highly influence its adsorptive potential. For instance, a well-developed microporous structure was reported as a key parameter to achieve high adsorption of formaldehyde molecules [13, 14].

One important aspect that needs to be considered when preparing biochar-based adsorbents is the particle size. In this regard, several studies have examined the relationship between the particle size and the adsorption performance of biochar materials in water and soil. For instance, Jin et al. [15] utilized biochar particles with different size ranges (up to 250 μm) for the removal of trichloroethylene from water. They reported that biochar with particle size under 75 μm exhibited higher adsorption capacity as compared to samples with bigger particle sizes. They attributed the results to an increase in specific surface area and micropore volume with a decrease in biochar particle size. Similarly, Han et al. [16] used magnetic biochar prepared from peanut hulls for the adsorption of Cr (VI) in aqueous media. They found that biochar's adsorption potential increased when the particle size decreased from 500-1000 μm to 150-500 μm, which was ascribed to the large surface area of small biochar particles. Another study [17] investigated the effect of millimeter, micron, and nanoscale biochar derived from corn straw and rice husk for the removal of diethyl phthalate from water. It was reported that the adsorption capacity of nanosized biochar particles was higher than the other samples. Findings were attributed to the well-developed porous structure of the nanosized biochar and suggested that the adsorption of the pollutant was assisted by a pore-filling mechanism rather than hydrogen bonding and noncovalent interactions. Regarding the application of biochar in contaminated soil remediation, prior research [18] showed that grinding biochar into smaller particle sizes did not change its pyrene removal efficiency. Likewise, Lebrun et al. [19] stated that biochar's particle size did not have a significant effect on soil properties and on As and Pb uptake.

The above literature suggests that the removal efficacy of pollutant by biochar with variable particle sizes might be different depending on the adsorption medium (i.e., water or soil). The evaluation of the particle size effect on the adsorptive potential of biochar in air seems to be interesting; however, only a few studies have addressed this topic. For example, Zhuang et al. [20] compared the VOC adsorption capacity of pristine and ball-milled biochar. They found that the size reduction of biochar by ball milling contributed to increasing the specific surface area and content in oxygen-containing functional groups which enhanced the adsorption capacity towards acetone and toluene.

Investigating a broad spectrum of biochar particle sizes will elucidate the influence of size on VOC adsorption capacity and identify potential changes induced by size reduction. A recent study [21] utilized three groups of microporous activated carbon with sizes ranging between 0.6 mm and 5 mm for benzene removal. Authors reported the dominant role of particle size on the adsorbed amount of benzene. They found that smaller activated carbon particles enhanced the adsorption process.

The objectives of this study were (i) to characterize the physical and structural properties of bark-derived biochar samples with variable particle size and (ii) to evaluate the effect of particle size on the adsorption efficiency of biochar towards formaldehyde and methanol with variable initial concentrations.

2. Materials and Methods

2.1. Materials and Reagents. A prechopped spruce (*Picea abies*) and pine (*Pinus sylvestris*) bark mixture was provided by Holmen (Stockholm, Sweden) for this study. Technical grade N_2 with a purity of 4.8 was used for the pyrolysis of the biomass and proximate analysis. High-grade N_2 and CO_2 gases with a purity of 5.0 were used for physisorption analysis. An aqueous formaldehyde solution (37% *v*/*v*, 30.03 g/mol) was purchased from CARLO ERBA reagents (DASIT group, Val de Reuil, France). Reagent grade methanol (purity ≥99.8%, 32.04 g/mol) was purchased from Honeywell (Riedel-de Haën, Seelze, Germany).

2.2. Preparation of Raw Bark Biomass. The bark material was comminuted with a cutting mill (Pulverisette 25/19, Fritsch, Idar-Oberstein, Germany) using a 4 mm mesh. The biomass was then subjected to a demineralization treatment by stirring the bark powder with distilled water (bark-water ratio equal to 1 : 10 *w*/*v*) at 60°C for 1 h. Subsequently, the material was drained, washed under a continuous flow of distilled water until reaching a neutral pH, and oven-dried at 105°C for 24 h. The demineralization was performed to reduce the ash content. Indeed, our previous work [22] indicated that decreasing the ash content in raw biomass enhanced the porosity of the prepared biochar. The ash content of the raw bark decreased from 3.02 ± 0.06% to 0.79 ± 0.02% after the demineralization process.

2.3. Preparation of Biochar Particles. The demineralized bark biomass was pyrolyzed in a tube furnace (RSRC 120-1000/13, Nabertherm, Lilienthal, *Germany*) for 30 min at 800°C. The pyrolysis was conducted under a nitrogen gas flow of 300 L/h and a heating rate of 1500°C/h. The pyrolysis conditions were selected based on preliminary optimization. Then, part of the obtained biochar powder was ball-milled in a planetary ball mill (Pulverisette 5, Fritsch, Idar-Oberstein, Germany) for 30 min at 400 rpm using stainless steel balls (20 mm in diameter) and distilled water. The ball-milled sample was then oven-dried overnight at 105°C and named "BM."

The remaining part of the biochar powder was ground using a benchtop grinder (IKA heavy-duty analytics, IKA, Staufen, Germany) and then sieved into six different groups with variable sizes using a sieve shaker (Minor M200, Endecotts, London, UK). Sieves with the following mesh sizes were used: 38 μm, 106 μm, 150 μm, 425 μm, 850 μm, and 1000 μm. Samples were labeled as P1, P2, P3, P4, P5, and P6, where the particle size increases from P1 to P6.

2.4. Characterization of the Biochar Particles. Particle size analysis was performed to investigate the size distributions of the biochar samples using a laser diffraction analyzer (LA-960A2, Horiba, Kyoto, Japan). Three repetitions were performed for each sample, and the average values were reported.

The volatiles, ash, and fixed carbon contents of the samples were determined by proximate analysis using a thermogravimetric analyzer (TGA801, LECO, Saint-Joseph, MI, USA). Analysis was performed according to the ASTM-D7582 standard. Three replicates were measured for each biochar, and the average values were determined and represented.

The surface morphology was evaluated using a field emission scanning electron microscope Carl Zeiss SUPRA 35 VP. Biochar samples were attached to SEM sample holders via double-sided carbon adhesive tape and sputtered with a thin layer of gold (Denton Vacuum LLC). Imaging was performed at an accelerating voltage of 1 kV and a working distance of approx. 4.5 mm. The crystallographic structure was evaluated using a Bruker D2 Phaser diffractometer (Cu–Kλ radiation; 1.5406 Å). Measurements were performed with a step size of 0.03° and a time/step of 1 s. Samples were dispersed in isopropanol, deposited on a Si zero background holder, and dried in order to obtain a thin layer of particles. XRD spectra were collected in the 2θ range from 5° to 80°.

The porosity evaluation was done using the physisorption technique (Anton Paar Quantachrome Instruments, Boynton Beach, Florida, USA). Samples were first degassed for 12 h at 250°C. The N_2 adsorption-desorption isotherms were obtained at 77 K and used to determine the specific surface area and pore volume according to the BET model. The meso- and macropore distributions were determined based on the BJH model. The CO_2 isotherms, obtained at 273 K, were used to investigate the microporous surface area, micropore volume, and size distribution according to the DFT model. Each sample was measured twice.

2.5. Adsorption Efficiency Tests. The adsorption efficiency of biochar samples with different particle sizes towards two different pollutants was evaluated in a batch experiment. Variable concentrations of pollutants (1, 2, and 3 ppm for formaldehyde and 10, 20, and 30 ppm for methanol) were injected in a sealed glass chamber where the biochar material was placed. The study involved investigating the fluctuation in pollutant concentrations over time, employing electrochemical gas sensors with a resolution of 0.1 ppm and a response time of 1 second: HCHO sensor (Stox-HCHO, EC Sense, Schäftlarn, Germany) and TVOC sensor (Stox-TVOC, EC Sense, Schäftlarn, Germany) for formaldehyde and methanol measurements, respectively. Continuous data acquisition was enabled by TVOC-HCHO logger software (ADDproS, Celje, Slovenia).

The adsorption efficiency (AE, %) was calculated according to equation (1), using the residual pollutant concentration measured in the chamber after 1 h, which was enough to reach the equilibrium phase.

$$\mathrm{AE}\,(\%) = \frac{C_0 - C_{1\mathrm{h}}}{C_0} \times 100, \tag{1}$$

where C_0 is the initial pollutant concentration (ppm) and $C_{1\mathrm{h}}$ is the pollutant concentration (ppm) measured after 1 h of the test. Three repetitions were performed for each sample, and the average values were reported.

2.6. Statistical Analysis. For statistical evaluation, one-way analysis of variance (ANOVA) was conducted using statistical software (SPSS Statistics v. 29, IBM Corp., Armonk, NY, USA). Significant differences among the mean values of the different biochar properties and adsorption efficiencies were determined using the Tukey post hoc test at a 5% significance level.

3. Results and Discussion

3.1. Particle Size Distribution. Average values and standard deviations of size distributions of the ball-milled (BM) and ground (P1-P6) biochar samples are listed in Table 1. Percentile values D_{10}, D_{50}, and D_{90} correspond to the size below which 10%, 50%, or 90% of all particles are obtained, respectively. The mean size indicates the average size value.

The particle size distributions of P1, P2, P3, and P4 samples were on the submillimeter scale while P5 and P6 had some particles above 1 mm (Table 1). The large standard deviation of values from P5 and P6 reflects the heterogeneity and high size variation within these fractions. This can be attributed to the differences in shapes and higher aspect ratios of biochar particles with the larger size. In this regard, Naito et al. [23] reported that rod-shaped particles (i.e., long particles) appeared in the wide size range when using the laser diffraction technique.

For the ball-milled sample, 50% of the particles were under 10 μm. Large particles were also detected ($D_{90} = 81 \pm 10$) in the BM fraction which likely resulted from the agglomeration of small particles. Longer ultrasonication time before measurement might be needed to prevent agglomeration and better

Table 1: Particle size representative diameters of the biochar samples.

Sample ID	D_{10} (μm)	D_{50} (μm)	D_{90} (μm)	Mean size (μm)
BM	3 ± 0	10 ± 0	81 ± 10	26 ± 2
P1	9 ± 0	22 ± 0	80 ± 9	44 ± 8
P2	34 ± 1	92 ± 33	111 ± 33	79 ± 0
P3	31 ± 2	103 ± 4	190 ± 2	109 ± 3
P4	48 ± 14	208 ± 20	423 ± 24	228 ± 21
P5	40 ± 12	403 ± 62	1459 ± 428	571 ± 58
P6	59 ± 1	731 ± 231	1860 ± 212	842 ± 102

Table 2: Proximate composition of bark-derived biochar particles.

Sample ID	Volatiles (%)	Ash (%)	Fixed carbon (%)
BM	13.20 ± 0.46a	10.40 ± 0.11a	74.8 ± 0.57a
P1	12.47 ± 0.50ab	5.33 ± 0.37b	79.58 ± 0.54b
P2	11.34 ± 0.42b	5.28 ± 0.14b	81.12 ± 0.45bc
P3	11.94 ± 0.60b	4.43 ± 0.20c	81.16 ± 0.70bc
P4	11.92 ± 0.51b	4.47 ± 0.52c	82.24 ± 0.82c
P5	12.77 ± 0.29a	4.71 ± 0.22bc	80.81 ± 0.77bc
P6	13.50 ± 0.35a	4.87 ± 0.19bc	80.02 ± 0.65b

Note: The results are expressed as mean ± standard deviation. Data in the same column with different letters were significantly different ($p < 0.05$).

represent the actual particle size. Using sieves for particle separation might not guarantee a completely homogeneous size in each fraction. In other words, it is assumed that all fractions can be eventually contaminated by particles of smaller size. Majka et al. [24] investigated the size distribution of beechwood dust particles. First, they separated different fractions by sieves, and then, they measured the content of the finest particles (<10 μm) using a laser technique. They found that each fine particle occurred in each fraction, and they concluded that the sieve method did not completely fractionate the samples into specific sizes. They explained that small particles were likely combined with the large ones due to electrostatic interactions.

3.2. Physical Composition. Results from the proximate analysis of the biochar samples with different particle sizes are shown in Table 2.

Volatiles, ash, and fixed carbon values ranged between 11% and 13%, 4% and 5%, and 79% and 82%, respectively (Table 2). All biochar samples had different compositions when compared with previously tested bark biochar materials [25, 26]. For instance, volatiles, ash, and fixed carbon contents were 25.90%, 17.90%, and 52.90% for Mallee tree bark biochar [25] and 24.07%, 17.68%, and 58.25% for Eucalyptus bark biochar [26], respectively. Differences between previous findings and this study might be related to the different pyrolysis conditions in which biochar samples were prepared (i.e., pyrolysis time and temperature). Moreover, the lower ash content of the biochar prepared in this study as compared to other reported data was expected considering that the raw biomass was demineralized before pyrolysis.

The physical composition (volatiles, ash, and fixed carbon) of biochar samples with different particle sizes was statistically significant ($p < 0.05$). However, major differences were observed between the ball-milled and ground samples. The volatile content decreased slightly and gradually with a decrease in particle size from P6 to P2 (from 13.5 ± 0.35% to 11.34 ± 0.42%). Then, it increased again when the size was further reduced from P2 to P1. The ash content remained almost steady for P3, P4, P5, and P6 samples.

However, the ash content was slightly high for P1 and P2 while it was considerably high for the ball-milled sample. The ash content increased by 96% for BM as compared to P1. The high ash content in the ball-milled sample could be a sign of contamination by inorganic iron metals released from the balls due to abrasion caused by high friction forces. Similar results were reported by Yuan et al. [27] who found that wet ball milling for 12 h increased the ash content of sawdust-derived biochar by 474% while size reduction by hand lapping did not affect the ash content. Another study [28] also reported that the ash content increased by 70% and 102% after ball milling of biochar for 12 h and 24 h, respectively. Authors reported that milling created some heat energy which dissipated and increased the temperature. Consequently, the biochar's composition changed. They concluded that the effect of increased ball milling time on biochar properties (including ash content) was comparable to the effect of increased pyrolysis temperature. The temperature increase during milling was stated to favor the volatilization of amorphous carbon leading to concentrating the ash components [28].

The fixed carbon content varied slightly among the ground biochar samples, and the values ranged between 79.58 ± 0.54% and 82.24 ± 0.82%. However, the BM sample had a significantly lower fixed carbon content of 74.8 ± 0.57% as compared to the ground samples. The same trend was observed in a prior study [27] where the carbon content decreased by 14.7% after wet ball milling which was ascribed to the dissolving and loss of organic carbon elements.

3.3. Morphological Properties of the Biochar Particles. SEM at different magnifications investigated the shape and surface morphology of the biochar samples with different particle sizes. Images are presented in Figure 1 (for a-g and h-n, the scale bar represents 100 μm and 1 μm, respectively).

As seen from the SEM images (Figure 1(g)), ball milling of pyrolyzed bark biomass produced the smallest particles with sizes smaller than the finest sieved product (P1, Figure 1(f)), as already shown with the particle size analysis (Table 1). While the BM sample population contains some larger pieces, it primarily consisted of fine dust particles. Sieving efficiently separated ground samples into six distinct size groups, comprising of rather heterogeneously shaped particles. As the particle size decreased, the coarse biochar particles with ordered block shapes (Figures 1(a)–1(c)) were transformed into finer particles with randomly disordered shapes (Figures 1(d)–1(g)). Indeed, the mechanical forces applied to the biochar particles during grinding and ball

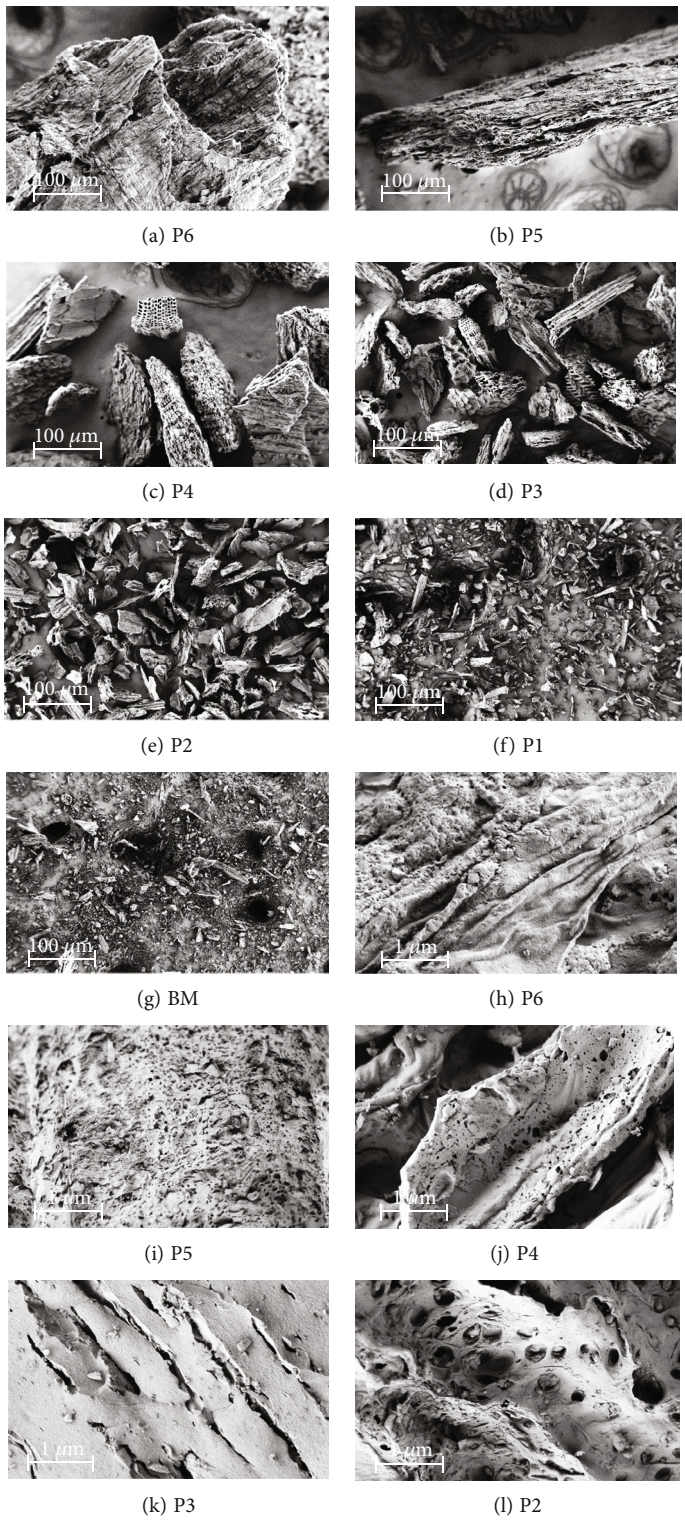

(a) P6 (b) P5

(c) P4 (d) P3

(e) P2 (f) P1

(g) BM (h) P6

(i) P5 (j) P4

(k) P3 (l) P2

Figure 1: Continued.

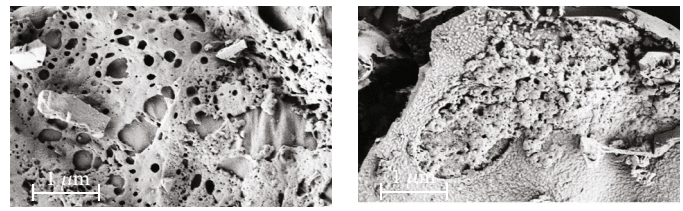

(m) P1 (n) BM

Figure 1: SEM images of the biochar samples with different particle sizes at different magnifications: (a–g) ×250, (h, k, m, n) ×25K, (i, l) ×10 K, and (h–n) ×15K.

milling processes led to the disruption of the internal bonds and modified the particles' structure. The size reduction was also associated with the occurrence of more pores that appeared progressively. In addition, changes in the shape of the pores were observed at higher magnification (Figures 1(h)–1(n)), specifically the transition from slit-shaped channels into round open pores.

The XRD patterns of the bark biomass particles and bark-derived biochar samples with different particle sizes are presented in Figure 2.

Raw bark with and without washing (i.e., demineralization before pyrolysis) exhibited typical diffraction patterns for cellulose-based biomass with sharper peaks stemming from crystalline lattice and broad region which is consistent with incoherent scattering from the amorphous phase. The most resolved peak at a scattering angle of approx. 22.6°, two broadened and overlapped peaks at approx.15.5° and 16.5°, and weak scattering at 34.9° angle correspond to Miller indices of (200), (1–10), (110), and (004), respectively, and are due to the Iβ cellulose, the most prominent scatterer in the bark/wood biomass. A large fraction of the diffuse scattering arises from amorphous constituents of bark biomass, like lignin. The only difference between diffractograms of unwashed and washed bark particles pertains to the higher intensity of the (200) reflection in washed bark samples, which could be due to the removal of water-soluble amorphous species, thus enhancing the overall crystalline diffraction signal. Despite the demineralization pretreatment, washed bark still exhibits the same sharp diffraction peak as the unwashed analogue, namely, at 2θ values of 15.6°, 24.9°, 27.7°, and 30.7° which closely match the scattering spectra of weddellite and whewellite, i.e., calcium oxalate [29]. Calcium oxalate, a biomineral form of Ca, synthesized by nearly all plants, is transformed into calcium carbonate ($CaCO_3$) above 400°C [30]. Upon inspection of diffraction patterns of the prepared biochar samples, only that of sample BM biochar exhibits characteristic peaks of calcite group carbonates (indexed with Crystallography Open Database (COD) 1010962), while scattering spectra of other samples (P1-P6) hardly contained peaks that could be ascribed to mineral phases; exceptions are samples P2 and P3 which display small peaks that can be attributed to SiO_2-containing minerals. In additional contrast to the BM sample, ground samples (P1-P6) still retain weak reflections of (110) and (004) crystallographic planes (of the bark's cellulose fraction) but shift to higher and smaller scattering angles, respectively, resulting in smaller and higher d-spacings above crystal planes. While these weak reflections still suggest some presence and reorganization of the cellulose fractions' crystalline structure, albeit to a very small degree, a complete disappearance of the (200) reflection for all biochar samples clearly shows that cellulose has undergone major thermal decomposition, as well as other poorly scattering bark constituents, as seen in a drastic decrease in the intensity of the amorphous part. It must be noted that the dismantling of the cellulose structural organization is a combined effect of thermal treatment and mechanical processing (ball milling has been shown to be more efficient in this regard).

In terms of conversion to carbon phase, all biochar samples exhibited three indicative broad peaks. Two broad diffraction peaks observed at around $2\theta = 9.5°$ and 43° (very slight) were attributed to the (002) plane which is a characteristic diffraction peak of graphene elements [31, 32]. The peak at around $2\theta = 18°$ assigned to the (002) plane reveals the amorphous structure of the biochar samples [31].

3.4. The Porosity of the Biochar Particles. The N_2 adsorption-desorption isotherms of the biochar samples are represented in Figure S1 (available in supplementary materials).

The N_2 adsorption-desorption isotherms can be classified as type I isotherm shape based on the IUPAC (International Union of Pure and Applied Chemistry) classification which is characteristic of carbonaceous materials with microporous structure. The BM sample exhibited the highest N_2 uptake (Figure S1a), suggesting that the ball milling treatment contributed to further expanding the porosity of the biochar material. The highest CO_2 uptake was obtained by the P6 (Figure S1b) sample which reveals the occurrence of more micropores in P6 as compared to other samples.

The BJH pore size distribution (Figure S2a available in supplementary materials) showed that the porosity was mainly composed of 5 nm and 10 nm mesopores for the ball-milled and ground biochar samples, respectively. Similarly, all biochar samples had comparable micropore distribution (Figure S2b) which was dominated by the presence of ultramicropores with sizes ranging between 0.3 nm and 0.8 nm.

The detailed porosity characteristics of the bark-derived biochar samples with different particle sizes are represented in Table 3.

The specific surface area and total pore volume of biochar samples increased gradually with the decrease in particle size. The specific surface area of P1 and BM was 102%

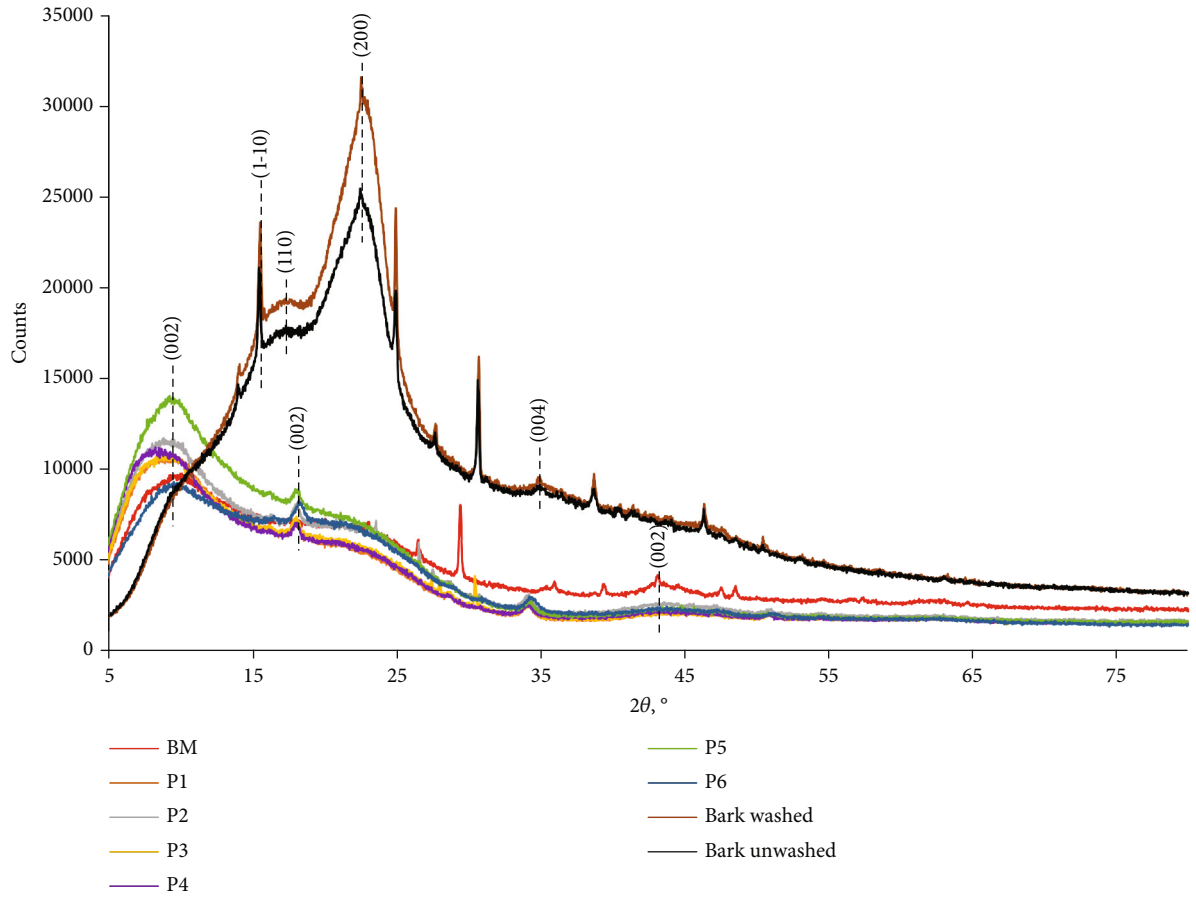

Figure 2: XRD patterns of raw bark and biochar samples with different particle sizes.

Table 3: Porosity evaluation of biochar samples with different particle sizes.

Sample ID	Specific surface area (m^2/g)	Total pore volume (cm^3/g)	Microporous surface area (m^2/g)	Micropore volume (cm^3/g)
BM	453.93 ± 0.50a	0.210 ± 0.004a	571.21 ± 0.50a	0.147 ± 0.001a
P1	333.758 ± 0.29b	0.172 ± 0.002b	597.22 ± 0.50b	0.155 ± 0.002ab
P2	313.823 ± 0.50c	0.267 ± 0.006c	622.53 ± 0.20c	0.162 ± 0.002b
P3	270.04 ± 0.50d	0.164 ± 0.002b	623.22 ± 0.250c	0.165 ± 0.003b
P4	254.072 ± 0.67e	0.140 ± 0.003d	612.17 ± 0.50d	0.161 ± 0.001b
P5	248.043 ± 0.40f	0.171 ± 0.002b	633.46 ± 0.30e	0.162 ± 0.001b
P6	224.446 ± 0.50g	0.142 ± 0.001d	658.01 ± 0.30f	0.179 ± 0.002c

Note: The results are expressed as mean ± standard deviation. Data in the same column with different letters were significantly different ($p < 0.05$).

and 48%, higher than P6. The ball-milled sample exhibited the largest specific surface area among other samples. Thus, the wet ball milling treatment enhanced the biochar's porosity more than the simple mechanical grinding. The reduction of particle size under the mechanical crushing effect (by grinding or ball milling) contributed to opening new pores and cavities and to reducing the grain size, which is in line with SEM observations (Figure 1). These changes enhanced the external and internal surface area, facilitating the adsorption of N_2 molecules (Figure 3(a)). The findings in this study are consistent with a prior study [27] where it was reported that specific surface area of biochar increased by 24% and 200% after hand grinding and ball milling, respectively. The effectiveness of ball milling in enhancing biochar's porosity was also confirmed by Zouari et al. [22]. It was found that specific surface area and pore volume significantly increased after wet ball milling for 30 min regardless of the biomass type (*Arundo donax* or olive stone) and biomass preparation method (with or without demineralization).

Interestingly, the changes in microporosity followed an opposite trend compared to the specific porosity results

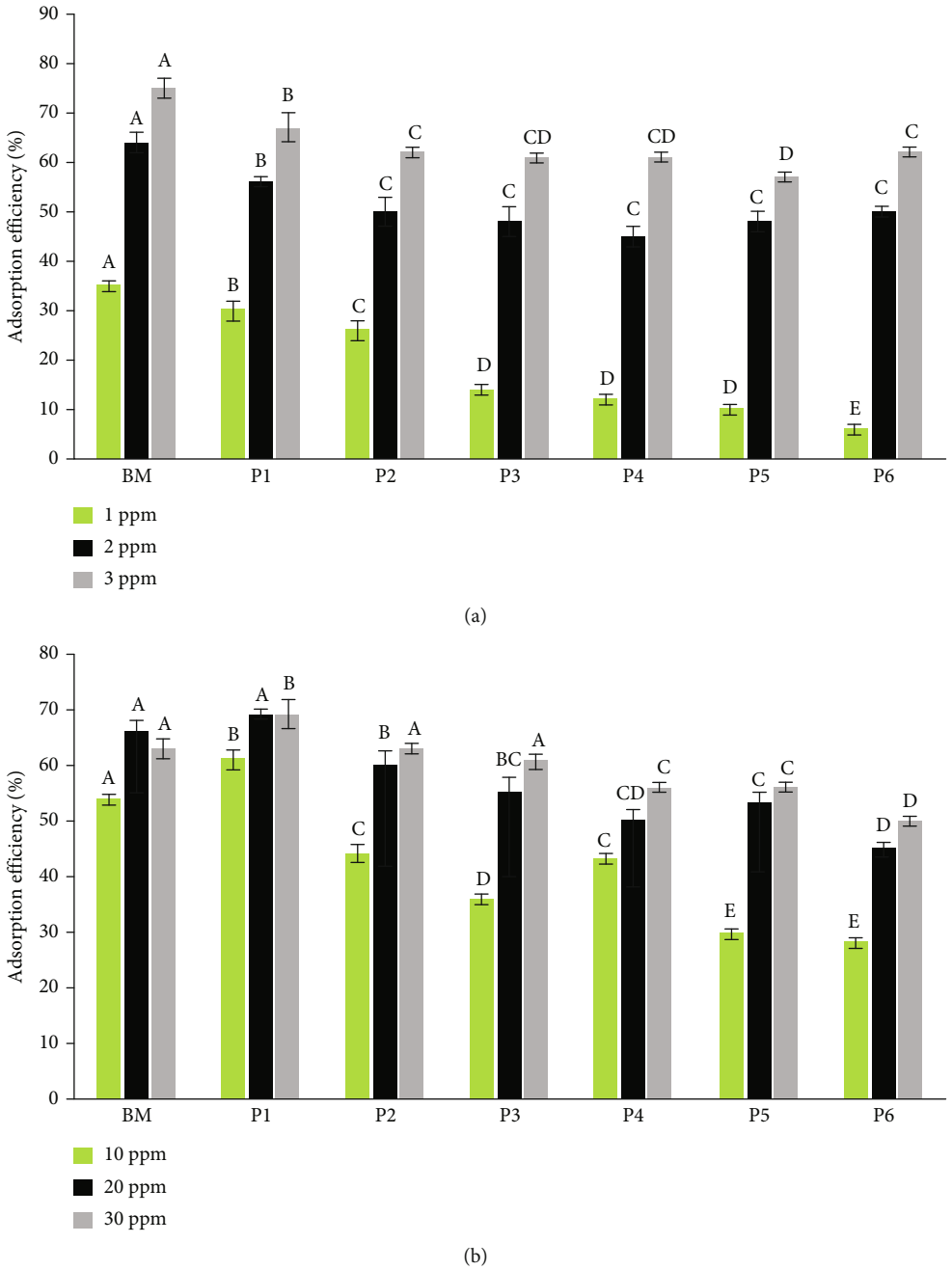

Figure 3: Adsorption efficiency of (a) formaldehyde and (b) methanol onto the biochar samples with different particle sizes. Results with different letters were significantly different ($p < 0.05$).

(Table 3). The microporous surface area and micropore volume decreased progressively with the decrease in particle size. The ball-milled sample had the lowest microporosity reflected by a 13% and 18% decrease in microporous surface area and micropore volume, respectively, as compared to P6. Size reduction via grinding and ball milling treatments likely contributed to the opening of the narrow pores in the pristine biochar. In other words, part of the micropores were widened under the mechanical crushing effect and fused to form larger pores (mainly mesopores) which led to decreasing the microporosity and increasing the specific surface area and total pore volume (Table 3). Similar results were reported previously [22] where wet ball milling induced a slight reduction in the microporosity of *Arundo donax*-derived biochar particles.

3.5. VOC Adsorption Efficiency of Biochar Particles. The formaldehyde and methanol adsorption efficiencies achieved after 1 h of experimental time by 1 g of biochar are presented in Figure 3.

All biochar samples exhibited a certain adsorption potential towards the tested VOCs regardless of the particle size and the initial pollutant concentration (Figure 3). The adsorption efficiencies of biochar samples ranged between

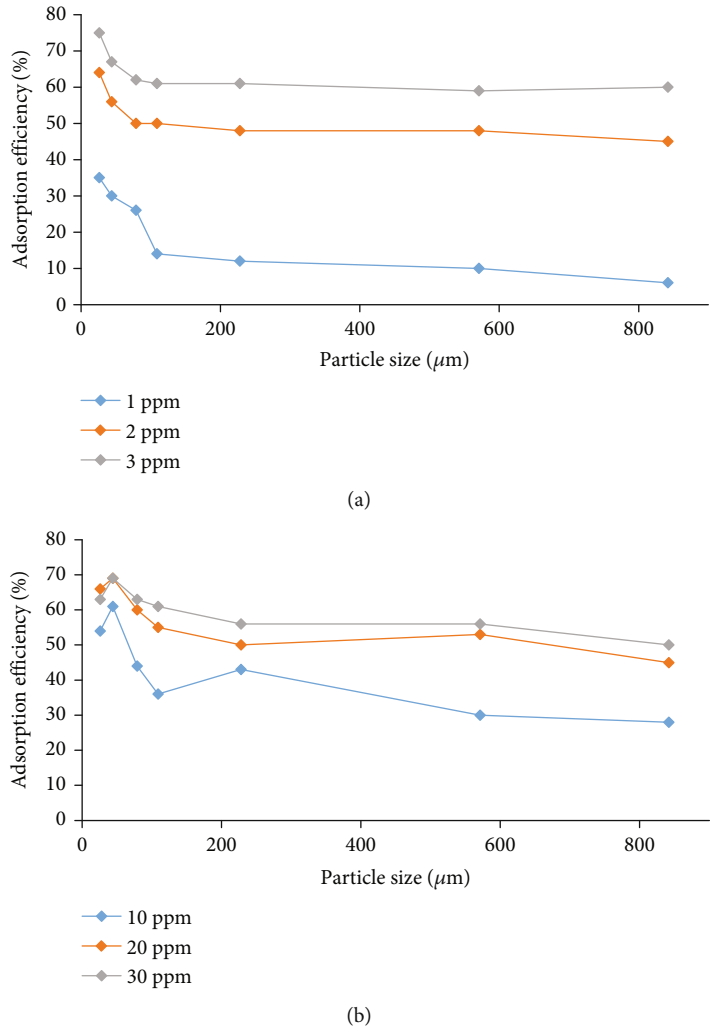

Figure 4: Effect of the particle size on the adsorption of (a) formaldehyde and (b) methanol onto the different biochar samples.

6% and 75% for formaldehyde and between 28% and 69% for methanol. The BM sample achieved the maximum formaldehyde adsorption efficiency at 35%, 64%, and 75% for 1 ppm, 2 ppm, and 3 ppm, respectively. Meanwhile, the P1 sample exhibited the maximum methanol adsorption capacity at about 61%, 69%, and 69% for 10 ppm, 20 ppm, and 30 ppm, respectively. The higher potential of smaller biochar particles in formaldehyde and methanol adsorption was attributed to their larger surface area and pore volume (Table 3) as compared to biochar particles with a larger size. Indeed, the well-developed porosity provided abundant adsorption sites for the pollutant molecules. Similarly, Ha et al. [21] reported that fine carbon particles (with a size under 0.6 mm) exhibited greater benzene uptake as compared to larger carbon particles (up to 5 mm in size) regardless of the pollutant flow rate.

To better understand the effect of biochar particle size on its adsorptive potential, the adsorption efficiency values were plotted in function of particle size and are represented in Figure 4.

Regarding the effect of particle size, a decrease in the adsorption efficiency with an increase in particle size was observed (Figure 4). The decrease in the adsorption capacity was observed in the group of samples with a smaller particle size (BM, P1, P2, and P3). However, the adsorption efficiencies were comparable for samples with larger particle sizes (P4, P5, and P6). This means that after a certain particle size value, about 200 μm in this case, further changes in the particle size did not significantly affect the biochar's adsorptive potential. Based on the statistical evaluation, less statistically significant values of adsorption efficiency were obtained within group P4, P5, and P6 (Figure 3).

The evolution of formaldehyde adsorption with the particle size was constant (Figure 4). However, in the case of methanol, the adsorption capacity of biochar with different particle sizes varied (Figure 4). This can be seen as a seemingly random increase and decrease in adsorption efficiency with increasing particle size. These results were attributed to the heterogeneity of the particle size distribution within the same sample. Another reason for this variation could be the presence of higher concentrations of methanol (10, 20, and 30 ppm) compared to formaldehyde (1, 2, and 3 ppm). In other words, the effect of particle size on the adsorption capacity at higher concentrations was less significant. To

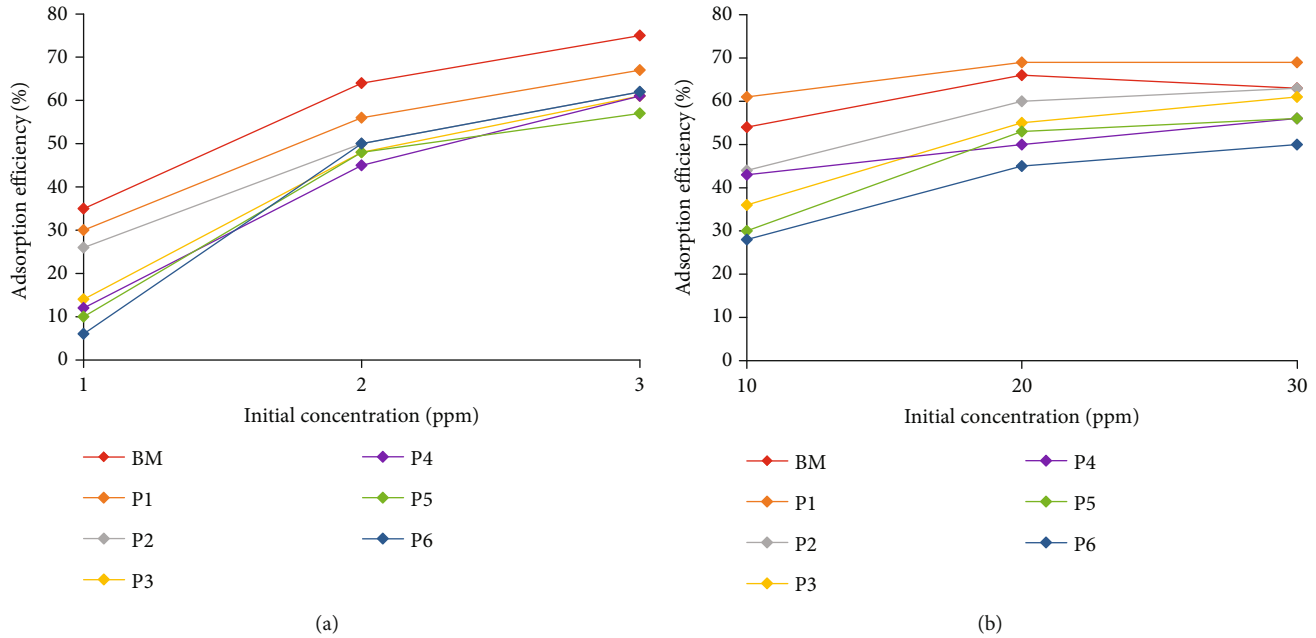

Figure 5: Effect of the initial concentration of the pollutants on the adsorption efficiency of (a) formaldehyde and (b) methanol onto the biochar samples.

confirm this assumption, the adsorption efficiencies of different samples were compared with the initial concentration of the pollutants and are shown in Figure 5.

The adsorption efficiency of both pollutants onto biochar increased with an increase in pollutant concentration (Figure 5). Hence, the adsorption of formaldehyde and methanol on the biochar samples was also dependent on their initial concentration. At higher initial concentrations, more pollutant molecules were present in the air phase which facilitated their contact with the biochar surface and enabled rapid access to the biochar pores. The adsorption process happens in three steps. First, pollutant molecules are transferred from the bulk air phase to the external surface of biochar particles. Then, the molecules diffuse into the porous structure of the biochar, and finally, they access the internal structure by the pore-filling effect. The presence of a high initial concentration of pollutants favors the first step in the adsorption process. Similar results were found by Hong et al. [33] when they investigated the adsorption of variable concentrations of VOC mixture on activated carbon fibers. They reported that the adsorption efficiency increased by 29% when the initial VOC concentration was increased from 200 mg/m^3 to 400 mg/m^3.

Interestingly, at 1 ppm of formaldehyde, the adsorption efficiency increased by 483% when the particle size decreased from P6 to BM, whereas at 3 ppm, the adsorption efficiency increased only by 21% with a decrease in particle size from P6 to BM. These results suggest that the impact of biochar particle size was less dominant when using biochar for the adsorption of high VOC concentrations. Considering that in the case of an application for the remediation of indoor air, where the VOCs usually occur at very low levels, it is preferable to utilize biochar with finer particle size.

The effect of contact time on the adsorption of formaldehyde and methanol with different initial concentrations was evaluated to estimate the time needed to reach equilibrium. Figure S3 (available in supplementary materials) represents the evolution of the adsorption efficiency of different biochar samples as a function of experimental time.

A gradual increase in the adsorption efficiency was observed as a function of time regardless of the sample size and the initial concentration of the pollutants (Figure S3). The adsorption rate was faster in the first 30 min. After that, the adsorption started to slow down to reach the equilibrium phase and stabilized by the end of the test. At the beginning of the experiment, the presence of available active sites (i.e., free pores) in the biochar material contributed to a faster adsorption rate. With the progress of the experimental time, the biochar pores were filled with formaldehyde or methanol molecules and reached saturation. After saturation, the biochar samples were not able to uptake more formaldehyde or methanol and the adsorption efficiency did not increase further. Similar results were reported on the adsorption of aromatic VOCs where the equilibrium time was reached after about 25 min [34].

It is worth noting that reaching the equilibrium state was achieved more rapidly for methanol adsorption tests. This was likely due to the high concentrations used for methanol (10, 20, and 30 ppm) as compared to formaldehyde (1, 2, and 3 ppm). At higher concentrations, more pollutant molecules were present in the surrounding air media which allowed faster contact with the adsorbent material (i.e., biochar) followed by the uptake in the biochar pores. Therefore,

vacant pores of biochar were quickly occupied, and the saturation phase was rapidly reached.

4. Conclusion

Spruce and pine bark were valorized through slow pyrolysis. Seven different samples of the obtained biochar with different particle sizes were prepared by ball milling or grinding and sieving. The biochar samples were used for the adsorption of differing concentrations of formaldehyde and methanol. The effect of particle size on the property of biochar and adsorption efficiency was examined.

The physical composition of the ground and sieved samples (P1 to P6) was similar. However, the ball-milled sample had higher ash content compared to other samples due to contamination of the biochar with iron likely generated from the metallic balls used in ball milling. XRD patterns revealed the occurrence of contamination peaks in the BM specimen spectra. Changes in pore structure and an increase in porosity were observed in SEM micrographs. The porosity of biochar increased with the decrease in particle size. The specific surface area and total pore volume of the ball-milled sample were 102% and 48% higher than P6, respectively. However, the microporosity decreased with the decrease in particle size which was attributed to the destruction and fusion of narrow pores during grinding or ball milling. All biochar samples were able to adsorb VOCs regardless of particle size and achieved an adsorption efficiency up to 75% for formaldehyde and 69% for methanol. Smaller particle size samples (BM and P1) exhibited high adsorption potential due to their well-developed porous structure. The adsorption efficiency also increased with the initial concentration of the introduced pollutant. The effect of biochar particle size on the adsorption efficiency was greater when a low concentration (1 ppm) of the pollutant was injected. However, at higher concentrations, biochar with different particle sizes showed comparable adsorption potential. Hence, for utilization in air remediation, the particle size of the biochar should be optimized with consideration of other factors such as amounts of the target pollutant.

This study addresses a common challenge in indoor environments and supports the development of a new class of biobased, sustainable, and functionalized products that improve human health through the improvement of indoor air quality. The findings from this study further the optimization of material production and tuning for application specific performance. The next step towards realizing the use of these BC particles for air remediation is through prototyping their application among commonly used consumer products, such as adhesives, coatings, and impregnates. We expect that these findings will further support greater uptake of biochar into the market as a high value-added product as well as a greater usage of underutilized, local, natural resources.

Data Availability

The data used to support the findings of this study are included within the supplementary information file.

Conflicts of Interest

The authors declare that they have no known competing financial interests or personal relationships that could have appeared to influence the work reported in this paper.

Authors' Contributions

Mariem Zouari contributed to the conceptualization, investigation, experimentation, and formal analysis of the study and wrote the original draft. Silvo Hribernik participated in the experimentation, formal analysis, and validation of the study. Matthew Schwarzkopf carried out the supervision, review, and editing of the study.

Acknowledgments

The authors gratefully thank and acknowledge the funding from the Slovenian Research and Innovation Agency for the projects N2-0225, J4-4546, and N2-0280. Furthermore, the authors thank the Slovenian Ministry of Higher Education, Research, and Innovation for funding the ForestValue Research Programme, specifically the project BarkBuild—tree bark as a renewable source of wood protection materials for building applications. Without the support of these projects related to biobased composite materials, we would not be able to generate high-quality research and researchers.

Supplementary Materials

The adsorption-desorption isotherms of biochar samples obtained from physisorption analysis under N_2 and CO_2 gases are represented in Figure S1. The pore size distribution obtained from N_2 analysis according to the BJH model and CO_2 analysis according to the DFT model are shown in Figure S2. The effect of the contact time on the adsorption efficiency of formaldehyde and methanol on the biochar samples is represented in Figure S3. *(Supplementary Materials)*

References

[1] WHO, "Household air pollution," December 2022, https://www.who.int/news-room/fact-sheets/detail/household-air-pollution-and-health.

[2] O. US EPA, "Volatile organic compounds' impact on indoor air quality," January 2024, https://www.epa.gov/indoor-air-quality-iaq/volatile-organic-compounds-impact-indoor-air-quality.

[3] L. Zhu, D. Shen, and K. H. Luo, "A critical review on VOCs adsorption by different porous materials: species, mechanisms and modification methods," *Journal of Hazardous Materials*, vol. 389, article 122102, 2020.

[4] C. Wehenkel, F. Cobos, A. Carrillo-Parra, and J. Lujan-Soto, "Estimating bark volumes for 16 native tree species on the Sierra Madre Occidental, Mexico," *Scandinavian Journal of Forest Research*, vol. 27, pp. 578–585, 2012.

[5] A. Thorenz, L. Wietschel, D. Stindt, and A. Tuma, "Assessment of agroforestry residue potentials for the bioeconomy in the European Union," *Journal of Cleaner Production*, vol. 176, pp. 348–359, 2018.

[6] R. Bauer, A. Billard, F. Mothe et al., "Modelling bark volume for six commercially important tree species in France: assessment of models and application at regional scale," *Annals of Forest Science*, vol. 78, no. 4, p. 104, 2021.

[7] U. Mantau, "Wood flow analysis: quantification of resource potentials, cascades and carbon effects," *Biomass and Bioenergy*, vol. 79, pp. 28–38, 2015.

[8] S. E. Corder, *Properties and uses of bark as an energy source*, Forest Research Laboratory, Oregon State University, 1976, February 2023, https://scholar.google.com/scholar_lookup?title=Properties+and+uses+of+bark+as+an+energy+source&author=Corder%2C+Stanley+E.&publication_year=1976.

[9] S. Feng, S. Cheng, Z. Yuan, M. Leitch, and C. Xu, "Valorization of bark for chemicals and materials: a review," *Renewable and Sustainable Energy Reviews*, vol. 26, pp. 560–578, 2013.

[10] J. Lehmann and S. Joseph, *Biochar for Environmental Management: Science, Technology and Implementation*, Routledge Taylor & Francis Group, London, UK, 2nd edition, 2015.

[11] X. Zhang, B. Gao, Y. Zheng et al., "Biochar for volatile organic compound (VOC) removal: sorption performance and governing mechanisms," *BioResource Technology*, vol. 245, pp. 606–614, 2017.

[12] P. Basu, "Chapter 5- pyrolysis," in *Biomass Gasification, Pyrolysis and Torrefaction (Second Edition), vol. Elsevier, Amsterdam, Netherlands*, P. Basu, Ed., pp. 147–176, Academic Press, Boston, 2013.

[13] N. R. Abdul Manap, R. Shamsudin, M. N. Maghpor, M. A. Abdul Hamid, and A. Jalar, "Adsorption isotherm and kinetic study of gas-solid system of formaldehyde on oil palm mesocarp bio-char: pyrolysis effect," *Journal of Environmental Chemical Engineering*, vol. 6, no. 1, pp. 970–983, 2018.

[14] M. Zouari, L. Marrot, and D. B. DeVallance, "Evaluation of properties and formaldehyde removal efficiency of biocarbon prepared at variable pyrolytic temperatures," *Frontiers in Environmental Science*, vol. 11, 2023.

[15] Z. Jin, S. Xiao, H. Dong et al., "Adsorption and catalytic degradation of organic contaminants by biochar: overlooked role of biochar's particle size," *Journal of Hazardous Materials*, vol. 422, article 126928, 2022.

[16] Y. Han, X. Cao, X. Ouyang, S. P. Sohi, and J. Chen, "Adsorption kinetics of magnetic biochar derived from peanut hull on removal of Cr (VI) from aqueous solution: effects of production conditions and particle size," *Chemosphere*, vol. 145, pp. 336–341, 2016.

[17] S. Ma, F. Jing, S. P. Sohi, and J. Chen, "New insights into contrasting mechanisms for PAE adsorption on millimeter, micron- and nano-scale biochar," *Environmental Science and Pollution Research*, vol. 26, no. 18, pp. 18636–18650, 2019.

[18] S. Hale, K. Hanley, J. Lehmann, A. Zimmerman, and G. Cornelissen, "Effects of chemical, biological, and physical aging as well as soil addition on the sorption of pyrene to activated carbon and biochar," *Environmental Science & Technology*, vol. 45, no. 24, pp. 10445–10453, 2011.

[19] M. Lebrun, F. Miard, N. Hattab-Hambli, G. S. Scippa, S. Bourgerie, and D. Morabito, "Effect of different tissue biochar amendments on As and Pb stabilization and phytoavailability in a contaminated mine technosol," *Science of the Total Environment*, vol. 707, article 135657, 2020.

[20] Z. Zhuang, L. Wang, and J. Tang, "Efficient removal of volatile organic compound by ball-milled biochars from different preparing conditions," *Journal of Hazardous Materials*, vol. 406, article 124676, 2021.

[21] S.-H. Ha, S. A. Younis, K. Vikrant, J. E. Szulejko, and K.-H. Kim, "Evidence of the dominant role of particle size in controlling the dynamic adsorption breakthrough behavior of gaseous benzene in a microporous carbon bed system," *Chemical Engineering Journal*, vol. 427, article 130977, 2022.

[22] M. Zouari, L. Marrot, and D. B. DeVallance, "Effect of demineralization and ball milling treatments on the properties of *Arundo donax* and olive stone-derived biochar," *International Journal of Environmental Science and Technology*, vol. 21, no. 1, pp. 101–114, 2024.

[23] M. Naito, O. Hayakawa, K. Nakahira, H. Mori, and J. Tsubaki, "Effect of particle shape on the particle size distribution measured with commercial equipment," *Powder Technology*, vol. 100, no. 1, pp. 52–60, 1998.

[24] J. Majka, M. Sydor, M. Pędzik et al., "Quantifying the finest particles in dust fractions created during the sanding of untreated and thermally modified beech wood," *BioResources*, vol. 17, no. 1, pp. 7–20, 2021.

[25] H. Abdullah, K. A. Mediaswanti, and H. Wu, "Biochar as a fuel: 2. Significant differences in fuel quality and ash properties of biochars from various biomass components of mallee trees," *Energy & Fuels*, vol. 24, no. 3, pp. 1972–1979, 2010.

[26] D. R. E. Padilla, L. R. O. Santos, D. A. Silva et al., "Eucalyptus bark charcoal: the influence of carbonization temperature in thermal behavior," *Materials Research*, vol. 22, 2019.

[27] Y. Yuan, N. Zhang, and X. Hu, "Effects of wet and dry ball milling on the physicochemical properties of sawdust derived-biochar," *Instrumentation Science & Technology*, vol. 48, no. 3, pp. 287–300, 2020.

[28] T. Wang, A. Rodriguez, M. Misra, and A. Mohanty, "Sustainable carbonaceous biofiller from Miscanthus: size reduction, characterization, and potential bio-composites applications," *BioResources*, vol. 13, 2018.

[29] I. H. Valido, J. M. Rius-Bartra, R. Boada, M. Resina-Gallego, M. Valiente, and M. López-Mesas, "Characterization of calcium oxalate hydrates and the transformation process," *ChemPhysChem*, vol. 21, no. 22, pp. 2583–2593, 2020.

[30] K. Jones, G. Ramakrishnan, M. Uchimiya et al., "Fate of higher-mass elements and surface functional groups during the pyrolysis of waste pecan shell," *Energy & Fuels*, vol. 29, no. 12, pp. 8095–8101, 2015.

[31] Y. Huang, E. Ma, and G. Zhao, "Thermal and structure analysis on reaction mechanisms during the preparation of activated carbon fibers by KOH activation from liquefied wood-based fibers," *Industrial Crops and Products*, vol. 69, pp. 447–455, 2015.

[32] L. Stobinski, B. Lesiak, A. Malolepszy et al., "Graphene oxide and reduced graphene oxide studied by the XRD, TEM and electron spectroscopy methods," *Journal of Electron Spectroscopy and Related Phenomena*, vol. 195, pp. 145–154, 2014.

[33] T. Hong, L. Wei, K. Cui et al., "Adsorption performance of volatile organic compounds on activated carbon fibers in a fixed bed column," *Journal of Environmental Chemical Engineering*, vol. 9, no. 6, article 106347, 2021.

[34] A. Aziz, M. Kim, S. Kim, and K. S. Kim, "Adsorption and kinetic studies of volatile organic compounds (VOCs) on seed assisted template free ZSM-5 zeolite in air," *Journal of Nanotechnology & Advanced Materials*, vol. 5, pp. 1–9, 2017.